

Simulation of enhanced characteristic x rays from a 40-MeV electron beam laser accelerated in plasma

L. Nikzad,^{1,*} R. Sadighi-Bonabi,² Z. Riazi,¹ M. Mohammadi,³ and F. Heydarian⁴

¹*Laser & Optics Research School, NSTRI, 14399-51113 Tehran, Iran*

²*Department of Physics, Sharif University of Technology, 11365-9567 Tehran, Iran*

³*Department of Physics, Khaje Nasir Toosi University of Technology, 1969764499 Tehran, Iran*

⁴*Department of Physics, Islamic Azad University, Central Branch, 14676-86831 Tehran, Iran*

(Received 27 November 2010; published 2 February 2012)

Simulation of x-ray generation from bombardment of various solid targets by quasimonoenergetic electrons is considered. The electron bunches are accelerated in a plasma produced by interaction of 500 mJ, 30 femtosecond laser pulses with a helium gas jet. These relativistic electrons propagate in the ion channel generated in the wake of the laser pulse. A beam of MeV electrons can interact with targets to generate x-ray radiation with keV energy. The MCNP-4C code based on Monte Carlo simulation is employed to compare the production of bremsstrahlung and characteristic x rays between 10 and 100 keV by using two quasi-Maxwellian and quasimonoenergetic energy distributions of electrons. For a specific electron spectrum and a definite sample, the maximum x-ray flux varies with the target thickness. Besides, by increasing the target atomic number, the maximum x-ray flux is increased and shifted towards a higher energy level. It is shown that by using the quasimonoenergetic electron profile, a more intense x ray can be produced relative to the quasi-Maxwellian profile (with the same total energy), representing up to 77% flux enhancement at K_{α} energy.

DOI: 10.1103/PhysRevSTAB.15.021301

PACS numbers: 52.38.Ph, 41.75.Ht, 41.50.+h

I. INTRODUCTION

Unlike optical radiation, x rays have the ability to penetrate optically opaque materials. The shorter wavelength (higher frequency) of x-ray sources with simultaneous high spatial and temporal resolutions has provided useful applications of x-ray imaging, diffraction, and spectroscopy in physics, chemistry, biology, medicine, and so on [1–4]. X rays have been generated via acceleration of electrons by different techniques, from ordinary x-ray generator tubes, and expensive huge accelerators, to recently developed laser-plasma accelerators [5–7] based on the development of chirped-pulse amplification (CPA) in laser systems [8]. In comparison with laser accelerators, more space, cost, and time to build along with the presence of complexity are inevitable to have a similar beam by conventional accelerators such as tubes and synchrotrons. The conventional systems can produce electron energy of more than 1 GeV in a storage ring with a diameter of 20–25 meters. However, generation of a GeV level of electron beam from a centimeter-scale accelerator is possible by means of intense lasers [9]. A detailed overview of research on new radiation sources using relativistic electrons can be found in [10].

Laser-plasma accelerators can produce high quality electrons with high energy and low beam divergence, which can be transported and focused easily, suitable in high resolution applications. The development of compact mode locked solid-state laser with short pulse, high peak power, and high repetition rate can be used to create electrons with almost the same pulse length and repetition rate. These accelerators are capable to provide electron beams with various energy profiles such as quasi-Maxwellian (q -Maxwellian) and quasimonoenergetic (q -monoenergetic) distributions. The created q -Maxwellian profile of electrons with very few accelerated electrons at high-energy levels has a great energy spread, limiting its use for potential applications. Under special conditions of plasma and laser pulses, it is possible to produce relativistic electron beams with a negligible divergence and a gradual energy spread [11]. The electron beam quality can be improved by selecting the appropriate interaction parameters of laser and plasma; particularly, by adjusting the interaction and dephasing lengths in the bubble regime, the formation of q -monoenergetic distribution of electrons is feasible [12–21]. During ultrashort intense laser-plasma interaction, the plasma electrons are trapped and accelerated to a single energy in the plasma bubble, generating an extremely collimated and q -monoenergetic electron beam. By irradiating gas jet targets with ultrashort pulses (less than 100 femtosecond) of high-power lasers (intensities of more than 10^{19} W/cm²) at high repetition rates, and for the plasma densities above the threshold (required for a breaking plasma wave), q -monoenergetic electron beams can be generated. Production of q -monoenergetic electrons by compact

*lida.nikzad@gmail.com

Published by the American Physical Society under the terms of the *Creative Commons Attribution 3.0 License*. Further distribution of this work must maintain attribution to the author(s) and the published article's title, journal citation, and DOI.

tabletop lasers is an important step forward in creating secondary radiations. One of the advantages of this possibility is related to outstanding progress in x-ray generation and its numerous crucial applications.

The laser produced electrons are suitable resources of x-ray generators with improved qualities such as higher energy levels and brightness, monochromaticity, compactness, flexibility, high repetition rate, high conversion efficiency, and short pulse duration. Furthermore, they are easily attainable in comparison with the conventional x-ray generators. These positive factors in x-ray diagnostics have been confirmed by using the Monte Carlo simulation [22]. While most sources of x rays provide a wide energy spectrum, it is now possible to produce nearly monochromatic [23], and possibly coherent x-ray beams, for instance by x-ray laser and free electron laser technologies [24,25]. Also, the sources of intense ultrashort x-ray pulses are accessible in laboratory scale [26–28]. X-ray beams can be generated by various approaches via irradiation of a laser beam on a target or by collision of laser pulses with accelerated electrons. For instance, Thomson scattering [29–33], Compton scattering [34,35], betatron oscillations [36–41], and high harmonic generation [42–46] are several methods of x-ray generation. Unlike the above-mentioned mechanisms of x-ray generation via direct laser-target interaction, in this paper the main attention is concentrated on an indirect scheme: First, electrons are produced by interaction of laser beam with a target; then the outgoing accelerated electrons collide with the second target creating x rays. During the electron-target interaction, electrons can be scattered from the nucleus, generating bremsstrahlung x-ray radiation, and also interact with inner-shell bound electrons of the material, creating characteristic x-ray radiation, due to decaying of outer electrons to the vacancies. At high energies (relativistic regime), bremsstrahlung x rays are emitted sharply straight in the forward direction with a continuous energy spectrum up to the impinging electron beam energy; while characteristic x rays are emitted isotropically with the femtosecond pulse duration, almost keeping that of the incident electron pulses.

The reported conversion efficiencies (x ray or electron to laser) have mostly been considered for direct laser-target interactions [26,47–50]. Analytical and numerical models have shown that an optimum laser intensity exists for maximum K_α yield, $I(\text{opt}) = 7 \times 10^9 Z^{4.4}$; moreover, for generating subpicosecond x-ray pulses, foil targets are better than bulks [51]. Also, for enhancing K_α x ray, laser irradiation of solid cones has been investigated instead of foils [52]. To increase the conversion efficiency of K_α x ray to laser, a novel two-stage target has been proposed, where by interaction of laser-primary foils, the most effective K_α -producing electrons are generated and transported into secondary x-ray converter foils [53].

Some investigations have been conducted about x-ray generation via electrons with various energy distributions. For example, continuum x-ray emission in inverse bremsstrahlung via non-Maxwellian electron spectrum [54], and x-ray generation by Maxwellian distributions [55] have been reported. Our main purpose is to study the role of electron energy profile on x-ray generation. Here, the production of bremsstrahlung and characteristic x rays is simulated by the interaction of two experimental energy spectra of electrons (q -monoenergetic and q -Maxwellian) with various thicknesses of lead, molybdenum, and tungsten targets. Then, the x-ray photons achieved by two electron spectra are compared at K_α energy (as the most prominent sources of characteristic x rays). It is found that between the outcomes achieved by these electron profiles with equal total energy, the results of the q -monoenergetic electron profile illustrate a considerable gain compared with the q -Maxwellian profile. For instance, the percentage increase of about 77% is attained by tungsten at its maximum measured thickness.

To the best of our knowledge, no devoted investigation has been reported with a scheme similar to this work, to be able to compare the results.

II. METHODOLOGY

In the present work, our simulation is performed by the MCNP-4C code based on the Monte Carlo approach [56], which has been attested as the most appropriate theoretical tool for calculation of x-ray spectra. Here, through the interaction of electrons with targets of various thicknesses, this code is employed for x-ray simulation to investigate the effect of electron energy distribution. The input file of the code contains different specification cards, including geometry card, source card, material card, and tally card. In the geometry card, the geometry of a subject is specified via the definition of surfaces and cells; in the source card, the source properties including its density, position, and the particle type (here electron) along with its direction and energy distribution are indicated; the specification of materials filling the various cells is introduced in the material card. At last, in the tally card, the output type is specified; in our work the tally type of F2 is activated to measure the average photon surface flux (per electron) in the selected energy range.

In laser-plasma interaction, the accelerated electrons pass through a target and interact with the atomic electrons and nuclei, leading to the emission of energetic characteristic and bremsstrahlung x-ray photons, with the maximum energy of the accelerated electrons. The radiation stopping power of electrons in a matter is given by [57]

$$\left(\frac{dE}{dx}\right)_{\text{rad}} = \frac{ZT(\text{MeV})}{750} \left(\frac{dE}{dx}\right)_{\text{ion}}, \quad (1)$$

where Z is the target atomic number and T is the electron energy, and $(dE/dx)_{\text{ion}}$, i.e., the ionization stopping power

during passing through a matter in the x direction, is introduced by the following equation:

$$\left(\frac{dE}{dx}\right)_{\text{ion}} \text{ (MeV/m)} = 4\pi r_0^2 \frac{mc^2}{\beta^2} NZ \left\{ \text{Ln} \left(\frac{\beta\gamma\sqrt{\gamma-1}}{I} mc^2 \right) + \frac{1}{2\gamma^2} \left[\frac{(\gamma-1)^2}{8} + 1 - (\gamma^2 + 2\gamma - 1) \text{Ln} 2 \right] \right\}. \quad (2)$$

In the above equation, $r_0 = e^2/mc^2 = 2.818 \times 10^{-15}$ (m) is the classical radius of electron, $mc^2 = 0.511$ MeV is the rest mass energy of electron, $\gamma = (1 - \beta^2)^{-1/2}$, $\beta = v/c$, where v and c are the electron and light velocities, respectively. Also, N is the number of atoms per unit volume, and I is the mean excitation potential of material which is in accordance with the approximate equation of $I(\text{eV}) = (9.76 + 58.8Z^{-1.19})Z$, for $Z \geq 12$. Paying attention to Eqs. (1) and (2), it can be seen that the radiation stopping power and the resulted x-ray photons in a target are dependent on the electrons and target specifications.

III. PHYSICAL SETUP TO BE SIMULATED

In our study, x-ray generation follows a two-step process: First, subsequent to the focusing of high intensity laser pulses on a supersonic He nozzle gas, plasma is produced and the accelerated electrons are emitted; next, as a result of the interaction of the MeV relativistic electrons with another solid target, they are converted to keV x-ray photons. In this paper, we focus on the latter step, i.e., the production of x-ray photons via the interaction of q -Maxwellian and q -monoenergetic electrons with solid targets including molybdenum (Mo), tungsten (W), and lead (Pb). The schematic of the experimental setup is shown in Fig. 1, where the first part of the setup corresponding to the q -monoenergetic electron generation is based on the earlier experimental work of our group [20]. A 20 TW, 30 fs Ti-sapphire CPA pulsed laser system at 10 Hz repetition rate is focused onto a He gas jet with a 2 mm cylindrical shape hole via a

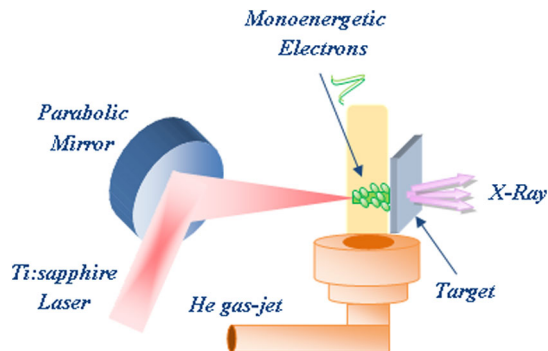


FIG. 1. A schematic of the experimental setup used for x-ray generation from a target irradiated by q -monoenergetic electrons due to laser-plasma interaction; the first part of this setup related to the q -monoenergetic electron generation is based on Ref. [20].

$f/5$ off-axis gold-coated parabolic mirror to generate a laser acceleration wakefield. For the laser power from 1 to 18 TW, and the plasma density from 2×10^{19} to $14 \times 10^{20} \text{ cm}^{-3}$, most of the produced electron energy spectra have q -Maxwellian distributions, while for the laser power of 16.6 TW (500 mJ) and the maximum plasma density of $14 \times 10^{19} \text{ cm}^{-3}$, at the laser focusing point of $250 \mu\text{m}$ from the nozzle edge and 1 mm above it, the q -monoenergetic feature is observed. All targets should be placed in the region where the generated bubbles or the q -monoenergetic electrons still subsist, i.e., up to about 1 mm after the laser focusing point on the gas jet.

The experimental q -Maxwellian and q -monoenergetic (say delta function) electron spectra achieved by different parameters of laser and plasma [20] are indicated in Fig. 2, where each electron energy distribution is an average of 100 pulses. The q -Maxwellian spectrum vastly distributed in the range of 0–12 MeV energy with the peak of about 1.5×10^7 (electron number $\text{MeV}^{-1} \text{ mSr}^{-1}$), achieved by the laser power of $P = 3.5$ TW and the He nozzle gas density of $3 \times 10^{19} \text{ cm}^{-3}$, is shown in Fig. 2 by the red dashed line. The q -monoenergetic spectrum spread from 30 to 48 MeV, with the energy peak of about 40 MeV and 1.24×10^7 (electron number $\text{MeV}^{-1} \text{ mSr}^{-1}$) with FWHM of 6.8 MeV, obtained by the laser power of $P = 16.6$ TW and the plasma density of $14 \times 10^{19} \text{ cm}^{-3}$, is also represented in Fig. 2 by the blue continued line. For more precise comparison of the results, these two electron profiles are considered with equal total energy amounts, i.e., electron number multiplied by average energy. The total energy of the q -monoenergetic profile is 1.46 times the reference Maxwellian profile. Thus, for the normalization process,

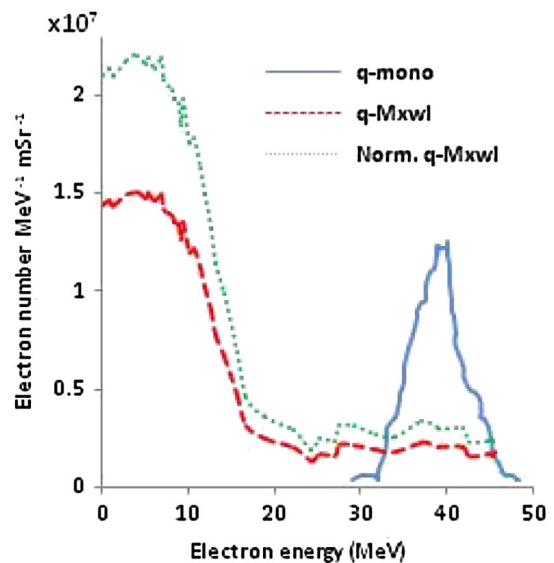


FIG. 2. The experimental electron distributions including the q -monoenergetic (blue continued line), the q -Maxwellian (red dashed line), and its normalized (green dotted line) plots are shown.

the electron number of the latter is multiplied by 1.46. The normalized q -Maxwellian profile is presented in Fig. 2 by the green dotted line. According to Fig. 1, the accelerated electrons with these two profiles are emitted towards the specific slabs of molybdenum ($Z = 42$), tungsten ($Z = 74$), and lead ($Z = 82$) with various thicknesses of about 100 to 3500 μm , in the normal direction. Afterward, the produced x-ray beam fluxes (photons number per unit area) including bremsstrahlung and characteristic radiations are determined in the energy domain of 10 to 100 keV by using the MCNP-4C simulation code. Finally, the properties of the x-ray spectra are discussed with respect to the thickness and the atomic number of the targets and also the energy distribution of the incident electrons. In all simulations, the number of incident electrons is selected so that the errors are less than 5%. It should be mentioned that the available experimental data of 40 MeV electrons, utilized here, do not indicate an optimum energy for x-ray production with keV energy.

IV. RESULTS AND DISCUSSION

The data of the experimental q -monoenergetic electron and the normalized q -Maxwellian electron spectra of Fig. 2 are employed to determine the output of x-ray data by the MCNP-4C simulation code. The outcomes obtained by these electron distributions are used to draw the x-ray spectra for three samples of Mo, W, and Pb, with the equal thickness of $d = 400 \mu\text{m}$, in one diagram for better comparison; refer to Fig. 3(a). It is clear that for each sample, the x-ray maximum flux (F_{max}) takes place at the same energy (E_{max}) (20 keV for Mo, 60 keV for W, and 75 keV for Pb), characterizing the material feature, and does not depend on the electron energy distribution. However, there are some differences in the attained magnitudes of F_{max} , representing that they do change with electron energy distribution. It should be noticed that although the total energies of the two electron profiles (the normalized q -Maxwellian and the q -monoenergetic) are arranged to be equivalent, the distribution patterns of electron number versus energy are different; therefore, they are expected to produce various x-ray fluxes. It can also be seen that by increasing the target atomic number (Z), F_{max} moves towards a higher energy amount, i.e., a larger E_{max} . Also, it can be seen that at this thickness, in the x-ray flux generated by the q -monoenergetic electron spectrum compared with the q -Maxwellian profile, there is an increase for Mo and a decrease for Pb; however, the difference in W is not noticeable. These results will be discussed later in Figs. 6 and 8(b), when the outcomes of these profiles are compared in various thicknesses.

By increasing the energy resolution, more characteristic x-ray peaks of K series are observable; this can be seen as an example for Pb in Fig. 3(b). The achieved maximum fluxes of x-ray photons produced in lead for all thicknesses are located at 75 keV, which is due to K_{α} ; at higher

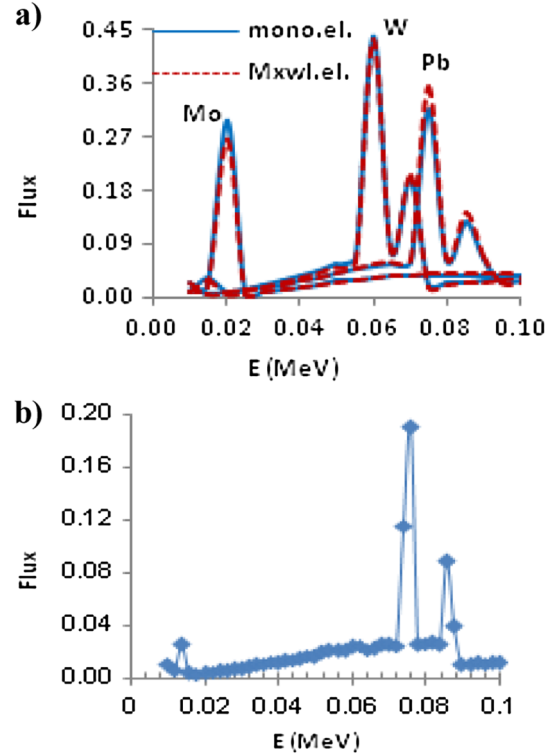


FIG. 3. (a) The production of x ray from the experimental q -monoenergetic and the normalized q -Maxwellian electrons of Fig. 2 by MCNP-4C code for three targets of Mo, W, and Pb with equal thicknesses of $d = 400 \mu\text{m}$; (b) the same as (a) for Pb with the q -monoenergetic electron profile, achieved by higher energy resolution, showing several characteristic peaks.

energy level a low peak is seen at $K_{\beta} \approx 86 \text{ keV}$ ($K_{\beta_1} = 84.9 \text{ keV}$, $K_{\beta_2} = 87.3 \text{ keV}$). Also, at a smaller energy amount of the spectrum, a low peak related to L series exists at 14 keV. These characteristic x rays are in good agreement with the experimental reports [58,59].

Since the x-ray flux varies with thickness in each target, the simulated x-ray data are achieved for several thicknesses. By applying the optimum thickness, d_{opt} , the maximum x-ray flux, F_{max} , is achieved at the energy level of E_{max} . The obtained results by using the q -Maxwellian and the q -monoenergetic electron profiles are illustrated in Figs. 4 and 5, respectively. It is apparent that d_{opt} and F_{max} alter with both factors of the target atomic number and the electron energy profile; although, E_{max} is constant for each material. Furthermore, it can be observed that by increasing the atomic number, the optimum thickness also increases. It can be recognized that for each sample, d_{opt} for the q -monoenergetic electron profile is larger than the q -Maxwellian one. According to Fig. 2, in the former, most electrons are accumulated on larger energy amounts compared with the latter, so they could pass through the larger thicknesses and produce the higher x-ray fluxes.

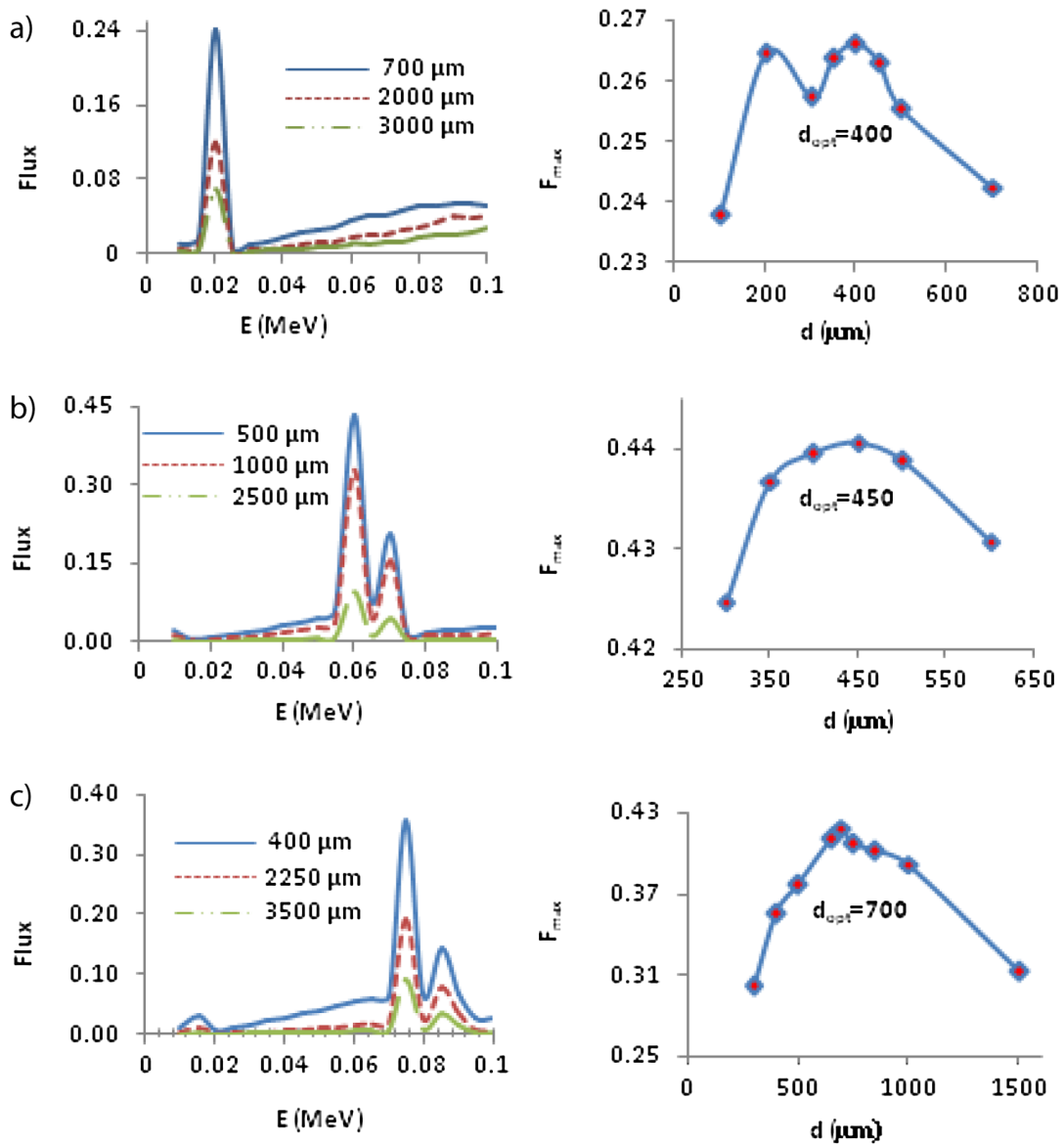


FIG. 4. The x-ray fluxes produced by the q -Maxwellian electron profile versus energy in several thicknesses (left), and the maximum x-ray flux versus thickness (right), for three targets (a) Mo, (b) W, and (c) Pb.

By finding the optimum thickness of each material for the two electron profiles, more exact comparison can be made on the x-ray fluxes at d_{opt} , shown in Fig. 6. Similar to Fig. 3, as it was mentioned before, for these electron distributions, E_{max} is the same for each specific target, but F_{max} alters. Moreover, it is perceived that by increasing the target atomic number, Z , the maximum of x-ray flux, F_{max} , moves towards higher energy level, i.e., higher E_{max} . Also, for W and Pb (with higher Z), the considerable growth of F_{max} is evident compared with Mo (with lower Z). Unlike Fig. 3, in this figure, the growth of x-ray production via the q -monoenergetic electron profile is obvious compared with the q -Maxwellian one, for all samples at the optimum thicknesses, d_{opt} .

From another point of view, the attained maxima of x-ray fluxes, F_{max} , are plotted for different materials, i.e., various atomic numbers, Z , in Fig. 7. It is revealed that the heavier samples of W and Pb with much higher Z (compared with Mo) illustrate the larger F_{max} in both electron profiles. However, it is noticeable that by using the q -monoenergetic electron profile, F_{max} is enlarged for each material in comparison with the q -Maxwellian profile.

At the next stage, more attention is paid to the evaluation of the x-ray fluxes magnitude (including bremsstrahlung and characteristic radiations) produced by the two electron profiles with the same energy at the K_{α} peak. It is shown that the x-ray flux produced by the q -monoenergetic

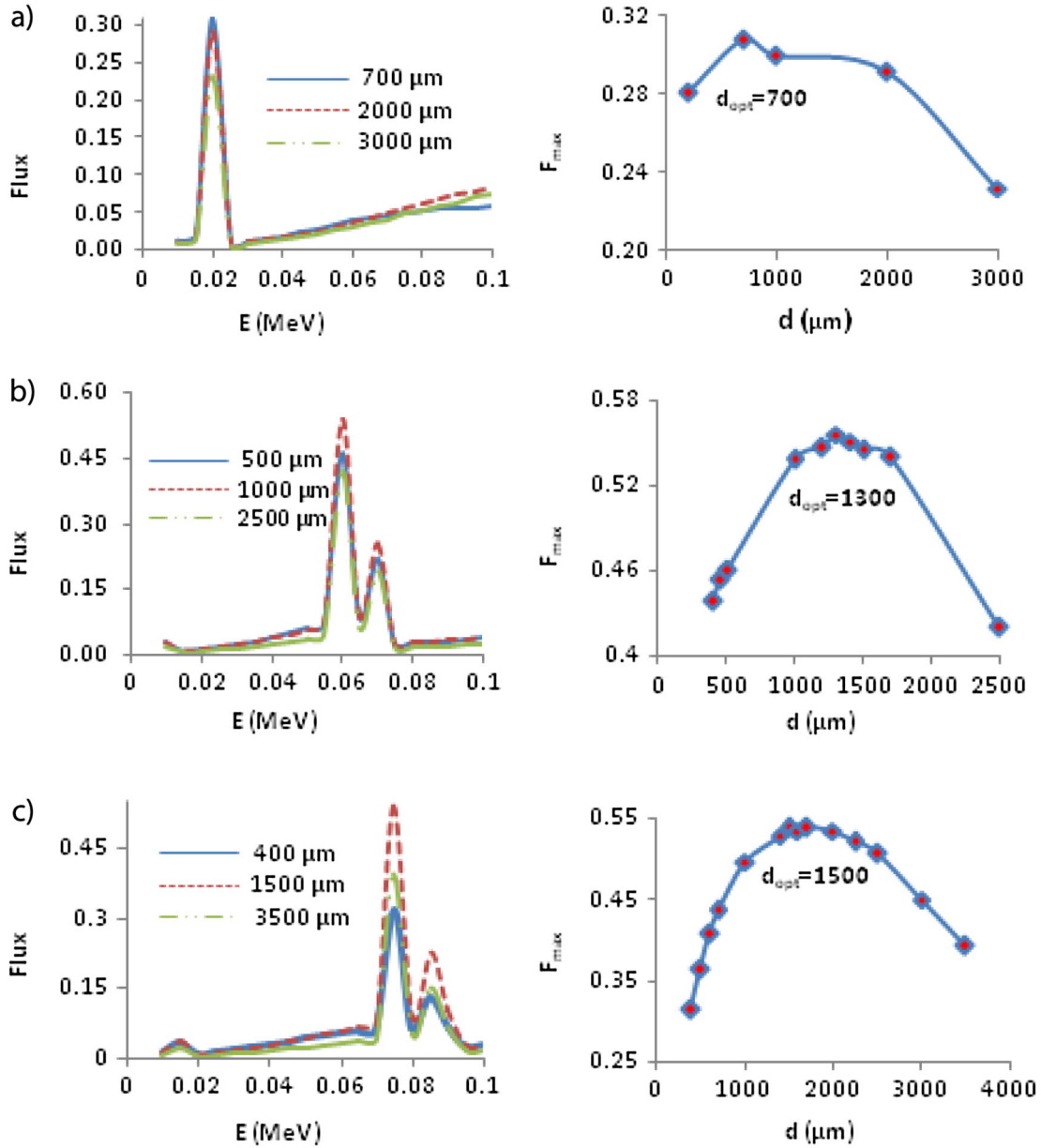


FIG. 5. The x-ray fluxes produced by the q -monoenergetic profile versus energy in several thicknesses (left), and the maximum x-ray flux versus thickness (right) for three targets (a) Mo, (b) W, and (c) Pb.

spectrum is higher than the one for the q -Maxwellian distribution. The percentage of increase is defined as $\Gamma = [(F_{\text{mono}} - F_{\text{Mxwl}})/F_{\text{mono}}] \times 100$, where F_{mono} and F_{Mxwl} stand for the x-ray fluxes produced by the q -monoenergetic and the q -Maxwellian electron distributions, respectively. In this paper, Γ (percentage of increase) is determined at the optimum thicknesses, d_{opt} , related to the profiles, and also at the maximum measured thickness (d_{max}). The outcomes for three samples of Mo, W, and Pb are presented in Table I. Similar to Figs. 4 and 5, it can be seen that for each target, d_{opt} obtained by the q -monoenergetic spectrum is larger than that of the q -Maxwellian one; also by increasing the target thickness, the difference between the two

created x-ray fluxes or Γ is enlarged. It is clear that, even by consideration of d_{opt} for the q -Maxwellian spectrum, the x-ray beam produced by the q -monoenergetic profile is still larger. It can be an evidence of providing the larger x-ray flux by the electrons with a q -monoenergetic nature compared with a q -Maxwellian one, specifically for the larger thicknesses. Practically, a q -monoenergetic distribution with much higher peak (more electrons) can be achieved by better adjustment of the laser focusing point on the gas jet, with the same laser power and the plasma density, resulting in Γ enlargement. As an example, this comparison can be observed in Fig. 8(a) for Pb with 1500 μm thickness, where about 42% gain is indicated in the

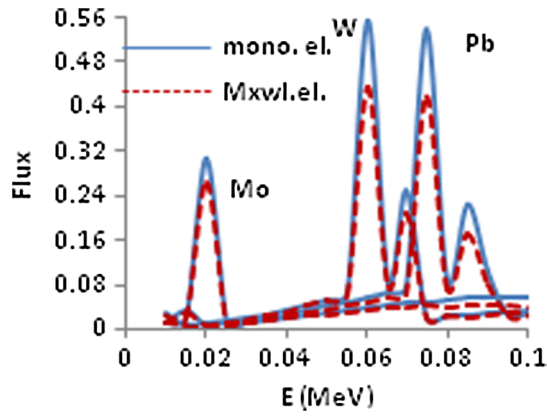


FIG. 6. The x-ray fluxes produced by the q -monoenergetic and the q -Maxwellian electron profiles at the optimum thickness, d_{opt} , of each target; for Mo, W, and Pb, they are 700, 1300, and 1500 μm , respectively, by the q -monoenergetic profile and they are 400, 450, and 700 μm , correspondingly, by the q -Maxwellian profile.

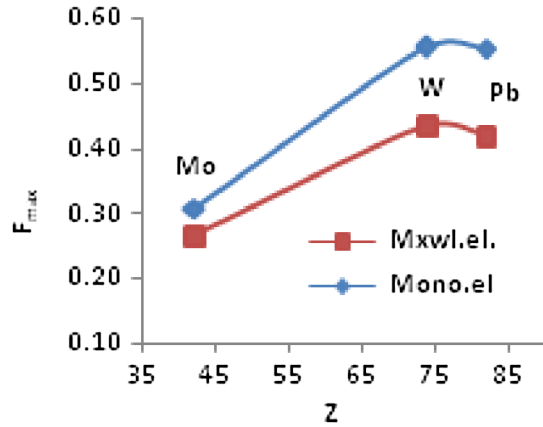


FIG. 7. A comparison of the x-ray fluxes maxima obtained by our experimental q -monoenergetic and q -Maxwellian electron distributions versus the atomic number, Z , for Mo ($Z = 42$), W ($Z = 72$), and Pb ($Z = 84$).

generated x-ray flux by using the q -monoenergetic electron distribution at the peak of $E = 75$ keV.

The relative ratio of the number of characteristic photons to bremsstrahlung photons in x-ray spectrum varies with the electron energy and the atomic number of the target. For the above-mentioned sample, the contributions of bremsstrahlung and characteristic x rays have been

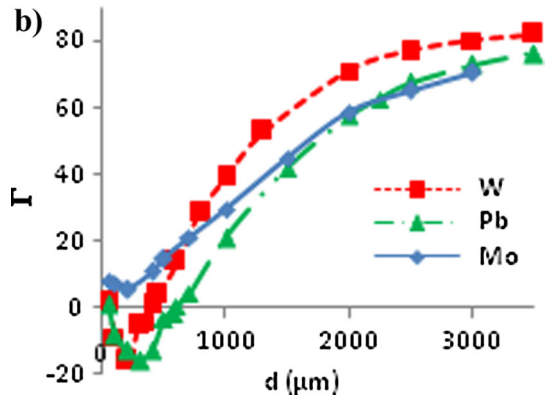
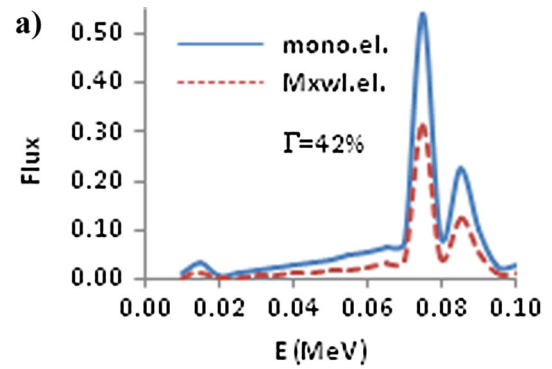


FIG. 8. (a) A comparison of the x-ray fluxes obtained by the q -monoenergetic and the q -Maxwellian electron distributions for Pb in $d = 1500$ μm , showing 42% percentage of increase by using the former compared with the latter. (b) Γ , percentage of increase of the x ray produced by the q -monoenergetic electrons compared with the q -Maxwellian electrons in different thicknesses for three targets of Mo, W, and Pb.

simulated, separately. It is revealed that their participations are 15.2% and 84.82%, respectively, by using the q -monoenergetic electrons and they are 13.34% and 86.66%, correspondingly, with the q -Maxwellian electrons; indicating a larger portion of the characteristic part at K_{α} energy. For instance, by using the q -monoenergetic electrons, from the total flux, i.e., 0.54 photons per area at 75 keV, the contribution of K_{α} characteristic radiation is 0.46 and the rest, i.e., 0.082 belongs to the bremsstrahlung share.

To investigate the thickness dependency of the percentage of increase, Γ , x-ray simulation has been performed for a large range of thicknesses. The results for three samples can be seen in Fig. 8(b). As this is shown, almost for all

TABLE I. A comparison of the x-ray flux percentage of increase, Γ , at the optimum thickness, d_{opt} , for each electron profile, and the maximum measured thickness, d_{max} , for three targets, (d is in micrometer).

Target	$d_{opt}^{Mxwl}(\mu\text{m})$	$\Gamma\%$	$d_{opt}^{mono}(\mu\text{m})$	$\Gamma\%$	$d_{max}^{measu}(\mu\text{m})$	$\Gamma\%$
Mo ($Z = 42$)	400	10.7	700	21.3	2500	65.35
W ($Z = 72$)	450	4	1300	53.14	2500	76.9
Pb ($Z = 84$)	700	4.5	1500	42.1	2500, 3500	67.66, 76.33

thicknesses, the q -monoenergetic electrons would produce more intense x-ray beams. However, there are a few exceptions in very low thicknesses of the higher Z samples of W and Pb where Γ becomes negative. In Fig. 8(b) the thicknesses of d_{\min} and d_0 are defined, respectively, at the minimum negative Γ (where the x-ray flux produced by the q -Maxwellian profile is in the most dominant status), and at $\Gamma = 0$ (with the equal x-ray fluxes created by the two profiles, where after that Γ becomes positive, i.e., x-ray flux produced by the q -monoenergetic profile prevails). It is seen that the quantities of d_{\min} and d_0 vary in different materials, and for the higher Z targets they are larger. Among our samples, Mo with the lowest Z shows positive Γ across the whole measured thicknesses and for W and Pb, Γ is positive after about 400, 600 μm , correspondingly. This is comparable with what is observed in Fig. 3(a) for x-ray evaluation by these electron profiles at relatively low thickness of 400 μm , where for Mo, W, and Pb, Γ represents positive, neutral, and negative trait, respectively. To explain the outcomes of Figs. 3(a) and 3(b), the nature of the electron energy spectra should be examined. According to Fig. 2, in the q -monoenergetic (q -Maxwellian) profile, a large number of electrons have been concentrated around higher (lower) energies, although the number of low-energy electrons in the wide energy spectrum of the q -Maxwellian profile is more. For x-ray generation from a high- Z material with small thickness, the q -Maxwellian profile is more appropriate, because the electrons with smaller energy amounts are capable to pass through a thin target and their larger number provides more x-ray photons. For a high- Z thick sample, more energetic electrons are needed to be able to pass through the material, revealing that the q -monoenergetic profile with almost all electrons focused around a large energy amount overcomes. While, the q -Maxwellian electrons may lose their lower energies in traversing a thick sample and be stopped. It is realized that for the higher Z targets of W and Pb, for $d > d_0$, Γ shows positive amounts, meaning that the q -monoenergetic profile is preferred. However, there is no such limitation for Mo as a low- Z material, in which the binding energy is higher and more energetic electrons are needed to generate x-ray photons; therefore, positive Γ is satisfied by the q -monoenergetic electron profile, even for smaller thicknesses.

It can be concluded that for x-ray generation from a high- Z target, the electron number plays a key role at small thickness, whereas the electron energy is the dominant factor at large thickness. As a result, in spite of the equal total energies of two spectra, the magnitudes of the created x-ray fluxes depend upon the distribution pattern of the electrons versus energy. It means that, in general, the accumulation of more electrons on higher energy levels plays an important role in the enhancement mechanism of photon generation.

V. APPLICATIONS AND SAFETY

A. X-RAY APPLICATIONS

There are various applications for bremsstrahlung and characteristic x rays. For example, the high-energy bremsstrahlung radiation is employed in radiotherapy and the lower energy part including the characteristic peaks is used for diagnostic imaging and material analyzing. Several medical applications of the laser-electron x-ray sources have been mentioned in Ref. [60]. The remarkable features of x-ray beam from laser-electron radiation source, such as monochromaticity, high intensity, tunability, directivity, and coherency have the main advantages in capturing images and x-ray diagnostics. The contrast among objects can be enhanced considerably by using monochromatic x rays instead of the common polychromatic spectra [61]. It is recognized that quasimonochromatic radiation could considerably improve the quality of the captured images and increase the precision of a 3D object reconstruction [62]. The characteristic K_α radiation has received full attention because of its potential as a monoenergetic, pulse x-ray source. Considering many applications of characteristic x-ray beam, many efforts have been made to produce a larger share of K_α radiation in comparison with bremsstrahlung emission. For example, by manipulating some parameters of laser and target, such as laser energy, prepulse, pulse duration, spot size, target thickness, and surface roughness, the production of K_α x rays can be optimized [63]. In fact, smaller radiating volumes emit brighter K_α radiation. The laser produced K_α is used as a probe in radiation biology [64]. Also, spectroscopic study of a K_α line is important to investigate the transport physics of hot electrons propagating in a dense material [65]. The emission of secondary characteristic x rays from a material or x-ray fluorescence can be used, for instance in elemental analysis during the study of building materials. The tunability of x rays is employed in material detection using near the K-edge transmission measurements [66], as well as in improvements to mammography configurations [67]. Furthermore, recent progress in ultrashort pulse generation technology has provided further possibilities for observation of ultrafast unknown phenomena. Several experiments have been introduced by using ultrashort x rays made of subpicosecond electron linac [68]. By employing an ultrafast (<100 fs) K_α x-ray source with suitable x-ray optics, a unique tool for studying subpicosecond phenomena over submicron scale lengths is possible. Ultrafast x rays enable us to capture a snapshot image of rapidly moving materials with high spatial and temporal resolutions. The multi-keV x ray is of major interest in the new fields of ultrafast x-ray diffractometry and biomedical radiography such as x-ray imaging for high-energy density physics [49,69]. Also, the creation of a bright, ultrafast laser-driven K_α x-ray source is used for observing time-resolved dynamics of atomic motion in solids and thin films [63]. This can also be used for time-resolved x-ray

scattering, the development of x-ray lasers [70], and ultra-fast, time-resolved x-ray diffraction [69,71].

B. SAFETY CONCERNS

The absorption of x rays by tissues can cause enormous damage to biological material. Therefore, x-ray doses should be controlled carefully and maximum limits should be placed to minimize the risks to patients and users, particularly in polychromatic x ray. It has been expressed that it is possible to simultaneously achieve a decrease in the surface radiation dose and in the total radiation dose of the patient and medical personnel without detriment to the instructiveness of diagnostic procedures [72]. By using x ray with higher energy and more directionality with reduced beam size, less scattered photons can occur. Utilization of monochromatic x ray also has advantages in reducing these hazards. In using characteristic x-ray radiation, K_α radiation is supposed to be maximized and high-energy bremsstrahlung (originated by MeV electrons) and the resulted ionizing radiation should be eliminated from the probe beam, depending on the conditions of the external object. This part of the emitted x ray in the forward direction presents a health hazard for the users of characteristic x rays, and may also confuse the interpretation of the effects. To shield these harmful radiations, the x-ray source can be housed in a vacuum vessel and surrounded by a Pb sheet to reduce the background of the scattered x rays. In general, by exploiting grids, filters, and collimators the harmful effects can be reduced. The shape, orientation, material, and thickness of an object will affect the absorption and thereby the angular distribution of the escaping x rays. To choose the best direction regarding the measurements and personnel security, the angular dependency of x-ray radiations should be taken into account. For high-energy electrons, bremsstrahlung radiation is strongly forward peaked in the electron direction and the backward emission is much smaller than that of the forward direction [68,73]. On the other hand, characteristic radiation is emitted isotropically [68,74], although an angular variation of the intensity is observed at the surface; this is caused by absorption of the radiation on its path through a target material [75]. Consequently, off-axis x rays (out of the incident electron beam line) can be used for the experiments focused on characteristic radiation. In this work, a similar angular dependency of x-ray intensity is shown by our simulation, for the normal entrance of electrons on a slab of Pb with $d = 1500 \mu\text{m}$. It is revealed that bremsstrahlung radiation is dominantly sharp in the straight and forward direction of electrons, and characteristic radiation is approximately isotropic with equivalent intensity in the forward and backward directions. As a result of this simulation, choosing an angle of about 100 degrees relative to the electron beam (in the backward direction) would be an appropriate direction of the probe x-ray beam for the characteristic x-ray users; provided that the suitable

positions for the object and measurement devices are feasible.

VI. CONCLUSION

In our simulation, the experimental q -monoenergetic electrons produced by laser-plasma interaction are employed to produce x-ray photons via collision with several targets. The results are compared with the simulated outcomes achieved by the observed q -Maxwellian electrons. These two experimental electron energy profiles are passed through three targets of molybdenum, tungsten, and lead with various thicknesses. X-ray simulation is performed by MCNP-4C code based on the Monte Carlo method in the energy range of 10 to 100 keV. It is shown that the produced x-ray spectrum depends on the electron energy distribution and the material characteristics. The results show that the maxima of the attained fluxes become greater by using the higher Z samples of tungsten and lead, and they locate at higher energies compared with the lower Z target of molybdenum. Also, by using different thicknesses and electron spectra for each target, the energy of which the maximum flux is produced remains unchanged, but the value of the maximum flux varies. The optimum thickness required for the optimum x-ray flux production is found for each target and each profile. The results reveal that two electron profiles with identical total energy can create different x-ray fluxes (including bremsstrahlung and characteristic x rays) at K_α energy. In low- Z materials for all thicknesses, d , and in high- Z materials for $d > d_0$ the q -monoenergetic electron profile produces more efficient x-ray photons, in comparison with the q -Maxwellian electron distribution. Concerning the influence of the two electron distributions on x-ray generation in high- Z targets, it is concluded that the presence of a larger number of electrons (even if distributed at lower energies) is more efficient at smaller target thicknesses, while the existence of electrons with higher energies (even fewer) is dominant at larger thicknesses. It is deduced that the accumulation of more electrons at higher energies in a q -monoenergetic spectrum with lower pulse width plays an important role in the increase of x-ray yield.

-
- [1] W. Chao, B. D. Harteneck, J. A. Liddle, E. H. Anderson, and D. T. Attwood, *Nature (London)* **435**, 1210 (2005).
 - [2] T. Ungár, in *Industrial Applications of X-Ray Diffraction*, edited by F. H. Chung and D. K. Smith (Marcel Dekker, Inc., New York, Basel, 2000).
 - [3] Y. Shvyd'ko, *X-ray Optics: High-Energy-Resolution Applications* (Springer-Verlag, Berlin, Heidelberg, 2004).
 - [4] J. Kirz, C. Jacobsen, and M. Howells, *Q. Rev. Biophys.* **28**, 33 (1995).
 - [5] T. Tajima and J. Dawson, *Phys. Rev. Lett.* **43**, 267 (1979).
 - [6] Nasr A. M. Hafz *et al.*, *Nature Photon.* **2**, 571 (2008).
 - [7] V. Malka *et al.*, *Nature Phys.* **4**, 447 (2008).

- [8] P. Maine *et al.*, *IEEE J. Quantum Electron.* **24**, 398 (1988).
- [9] W. P. Leemans *et al.*, *Nature Phys.* **2**, 696 (2006).
- [10] P. Rullhusen, X. Artru, and P. Dhez, *Novel Radiation Sources Using Relativistic Electrons: From Infrared to x-rays* (World Scientific, Singapore, 1998).
- [11] C. G. R. Geddes *et al.*, *Nature (London)* **431**, 538 (2004).
- [12] A. Pukhov and J. Meyer-ter-Vehn, *Appl. Phys. B* **74**, 355 (2002).
- [13] S. P. D. Mangles *et al.*, *Nature (London)* **431**, 535 (2004).
- [14] J. Faure *et al.*, *Nature (London)* **431**, 541 (2004).
- [15] I. Kostyukov, A. Pukhov, and S. Kiselev, *Phys. Plasmas* **11**, 5256 (2004).
- [16] V. Malka, J. Faure, A. Pukhov, and J. P. Rousseau, *Phys. Plasmas* **12**, 056702 (2005).
- [17] Y. Glinec *et al.*, *Laser Part. Beams* **23**, 161 (2005).
- [18] K. Krushelnick *et al.*, *Phys. Plasmas* **12**, 056711 (2005).
- [19] Z. L. Chen *et al.*, *Laser Part. Beams* **26**, 147 (2008).
- [20] R. Sadighi-Bonabi, H. A. Navid, and P. Zobdeh, *Laser Part. Beams* **27**, 223 (2009).
- [21] R. Sadighi-Bonabi and Sh. Rahmatollahpur, *Phys. Rev. A* **81**, 023408 (2010).
- [22] A. M. Gurvich, *Physical Fundamentals of Radiation Control and Diagnostics* (Energoatomizdat, Moscow, 1989).
- [23] F. E. Carroll, M. H. Mendenhall, R. H. Traeger, C. Brau, and J. W. Waters, *Am. J. Roentgenol.* **181**, 1197 (2003).
- [24] S. V. Milton *et al.*, *Science* **292**, 2037 (2001).
- [25] I. A. Vartanyants *et al.*, *Phys. Rev. Lett.* **107**, 144801 (2011).
- [26] J. D. Kmetec *et al.*, *Phys. Rev. Lett.* **68**, 1527 (1992).
- [27] M. Yoshida, Y. Fujimoto, Y. Hironaka, K. G. Nakamura, K. Kondo, M. Ohtani, and H. Tsunemi, *Appl. Phys. Lett.* **73**, 2393 (1998).
- [28] J. C. Kieffer *et al.*, *Phys. Fluids B* **5**, 2676 (1993).
- [29] R. W. Schoenlein *et al.*, *Science* **274**, 236 (1996).
- [30] M. Babzien *et al.*, *Phys. Rev. Lett.* **96**, 054802 (2006).
- [31] S. Y. Chen, A. Maksimchuk, and D. Umstadter, *Nature (London)* **396**, 653 (1998).
- [32] K. Ta Phuoc *et al.*, *Phys. Rev. Lett.* **91**, 195001 (2003).
- [33] H.-C. Wu *et al.*, *Phys. Rev. ST Accel. Beams* **14**, 070702 (2011).
- [34] C. Pellegrini, *J. X-Ray Sci. Technol.* **4**, 275 (1994).
- [35] C. Sun and Y. K. Wu, *Phys. Rev. ST Accel. Beams* **14**, 044701 (2011).
- [36] E. Esarey, B. A. Shadwick, P. Catravas, and W. P. Leemans, *Phys. Rev. E* **65**, 056505 (2002).
- [37] I. Kostyukov, S. Kiselev, and A. Pukhov, *Phys. Plasmas* **10**, 4818 (2003).
- [38] A. Rousse *et al.*, *Phys. Rev. Lett.* **93**, 135005 (2004).
- [39] S. Kiselev, A. Pukhov, and I. Kostyukov, *Phys. Rev. Lett.* **93**, 135004 (2004).
- [40] F. Albert *et al.*, *Phys. Rev. E* **77**, 056402 (2008).
- [41] A. G. R. Thomas and K. Krushelnick, *Phys. Plasmas* **16**, 103103 (2009).
- [42] M. Drescher *et al.*, *Science* **291**, 1923 (2001).
- [43] I. McKinnie and H. Kapteyn, *Nature Photon.* **4**, 149 (2010).
- [44] P. M. Paul *et al.*, *Science* **292**, 1689 (2001).
- [45] A. Baltuška *et al.*, *Nature (London)* **421**, 611 (2003).
- [46] J. Seres *et al.*, *Nature (London)* **433**, 596 (2005).
- [47] S. C. Wilks and W. L. Kruer, *IEEE J. Quantum Electron.* **33**, 1954 (1997).
- [48] S. J. Pestehe, G. J. Tallents, I. C. E. Turcu, Y. Abou Ali, G. Hirst, M. Powers, and W. Shaikh, *J. Phys. D* **35**, 1117 (2002).
- [49] *Applications of Laser Plasma Interactions*, edited by Shalom Eliezer and Kunioki Mima (Taylor & Francis, London, 2009).
- [50] A. Rousse *et al.*, *Phys. Rev. E* **50**, 2200 (1994).
- [51] C. Reich, P. Gibbon, I. Uschmann, and E. Forster, *Phys. Rev. Lett.* **84**, 4846 (2000).
- [52] XiaoYa Li *et al.*, *Phys. Rev. E* **83**, 046404 (2011).
- [53] A. B. Sefkow, *Phys. Rev. Lett.* **106**, 235002 (2011).
- [54] J. P. Matte *et al.*, *Plasma Phys. Controlled Fusion* **30**, 1665 (1988).
- [55] G. H. McCall, *J. Phys. D* **15**, 823 (1982).
- [56] MCNPTM—A General Monte Carlo N-Particle transport Code, edited by J. F. Briesmeister (Version 4C, Los Alamos National Laboratory, LA-13709-M, 2000).
- [57] G. F. Knoll, *Radiation Detection and Measurement* (John Wiley & Sons, Inc., New York, 2000), 3rd ed.
- [58] J. W. Robinson, *Handbook of Spectroscopy* (CRC Press, Cleveland, 1974), Vol. 1, p. 228.
- [59] S. I. Salem, S. L. Panossian, and R. A. Krause, *At. Data Nucl. Data Tables* **14**, 91 (1974).
- [60] E. G. Bessonov, A. V. Vinogradov, and A. G. Tourianskii, *Instrum. Exp. Tech.* **45**, 718 (2002).
- [61] F. E. Carroll, *Am. J. Roentgenol.* **179**, 583 (2002).
- [62] G. T. Herman, *Image Reconstruction from Projections: The Fundamentals of Computerized Tomography* (Academic, New York, 1980).
- [63] C. W. Siders *et al.*, Report No. UCRL-TR-228409, FY06 LDRD Final Report, Tracking Code: 04-ERD-064, 2007.
- [64] M. Nishikino *et al.*, *Rev. Sci. Instrum.* **81**, 026107 (2010).
- [65] K. B. Wharton *et al.*, *Phys. Rev. Lett.* **81**, 822 (1998).
- [66] F. Hagenbuck *et al.*, *IEEE Trans. Nucl. Sci.* **48**, 843 (2001).
- [67] M. A. Piestrup, X. Wu, V. V. Kaplan, S. R. Uglov, J. T. Cremer, D. W. Rule, and R. B. Fiorito, *Rev. Sci. Instrum.* **72**, 2159 (2001).
- [68] H. Harano *et al.*, *J. Nucl. Mater.* **280**, 255 (2000).
- [69] C. Rischel *et al.*, *Nature (London)* **390**, 490 (1997).
- [70] M. M. Murnane *et al.*, *Science* **251**, 531 (1991).
- [71] C. Rose-Petruck *et al.*, *Nature (London)* **398**, 310 (1999).
- [72] V. P. Mashkovich, *Zashchita ot ioniziruyushchikh izlucheni: Spravochnik (Protection against Ionizing Radiation: A Handbook)* (Energoatomizdat, Moscow, 1982).
- [73] B. S. Rao *et al.*, *J. Appl. Phys.* **102**, 063307 (2007).
- [74] A. A. Shaltout, *Eur. Phys. J. Appl. Phys.* **37**, 291 (2007).
- [75] M. Green, *Proc. Phys. Soc.* **83**, 435 (1964).